Journal of Alloys and Compounds 509 (2011) 10211–10216

Contents lists available at SciVerse ScienceDirect

Journal of Alloys and Compounds

journal homepage: www.elsevier.com/locate/jallcom

Magnetic and photoluminescence properties of Fe_3O_4@SiO_2@$YP_{1-x}V_xO_4$:Dy^{3+} nanocomposites

Jianhui Shi, Deming Liu, Lizhu Tong, Xuwei Yang, Hua Yang*

College of Chemistry, Jilin University, Changchun, 130012, China

ARTICLE INFO

Article history:
Received 25 June 2011
Received in revised form 15 August 2011
Accepted 17 August 2011
Available online 25 August 2011

Keywords:
Coating materials
Composite materials
Phosphors
Magnetically ordered materials
Nanofabrications
Optical properties

ABSTRACT

In this paper, we report on the bifunctional Fe_3O_4@SiO_2@$YP_{0.1}V_{0.9}O_4$:Dy^{3+} nanocomposites were prepared by the solvothermal method and sol–gel method. The structure, photoluminescence (PL) and magnetic properties of the nanocomposites were characterized by means of X-ray diffraction, scanning electron microscope, transmission electron microscope, PL excitation and emission spectra and vibration sample magnetometry. It is shown that Fe_3O_4@SiO_2@$YP_{0.1}V_{0.9}O_4$:Dy^{3+} nanocomposites with a core–shell structure present excellent fluorescent and magnetic properties. Additionally, the effects of the magnetic field on the luminescence properties of nanocomposites were discussed.

1. Introduction

In recent years, the application of photoluminescence (PL) and magnetic nanocomposites have advanced development of bioimaging technologies [1,2]. The integration of fluorescent properties and magnetic properties further offers a new potential application for in vitro and in vivo imaging. Magnetic-fluorescent nanoparticles serve both as magnetic resonance contrast agents for magnetic resonance imaging (MRI) and drug delivery agents, as well as in cell separation and labeling [3,4] and optical probes for intravital fluorescence microscopy [5].

Most nanocomposites-based optical imaging agents can be subdivided into two categories: quantum dots (QDs) and dye-doped nanoparticles [1,6]. Usually, QDs are photochemically stable [7] and have narrow, tunable emission spectra [8], and are metabolically stable [9]. However, issues of toxicity (generally related to heavy metal ions such as Pb^{2+} or Cd^{2+}), photo-oxidation, and difficult surface conjugation chemistry associated with QDs limit its applications, and a protective shell of insulating material or semiconductor is introduced to overcome these problems [10], which indeed complicates the fabricating process. But for dye molecules, they suffer from photobleaching and quenching due to interactions with solvent molecules and reactive species such as oxygen or ions dissolved in solution when they are exposed to a variety of harsh environments [11,12].

Most recently, new photostable materials derived from lanthanide-doped nanoparticles have begun to gain attraction due to its excellent luminescence properties, including large Stokes shifts, high quantum yields, long lifetimes and superior photostability [6,13]. The presented examples include γ-Fe_2O_3/$NaYF_4$:Y, Er nanoparticles [14], Co:Nd:Fe_2O_3/Gd_2O_3:Eu core-shell particles [15], Tb-doped γ-Fe_2O_3 nanocrystals [11], Fe_3O_4@Y_2O_3:Eu nanocomposites [6], Fe_3O_4@YPO_4:Re (Re = Tb, Eu) [16] and Fe_3O_4@YVO_4:Eu nanocomposites [17]. Although there have been already some reports on composites based on magnetite and lanthanide dopants or lanthanide complexes [18], to the best of our knowledge, there are no previous reports detailing the synthesis of bifunctional nanocomposites Fe_3O_4@SiO_2@$YP_{0.1}V_{0.9}O_4$:Dy^{3+} components in general.

2. Experimental details

2.1. Materials

Ferrous chloride hexahydrate ($FeCl_3{\cdot}6H_2O$) (99%) were purchased from Alfa Aesar Co. Y_2O_3 (99.9%) and Dy_2O_3 (99.9%) were purchased from BeiJing chemical plant. Sodium hydroxide (NaOH), ammonium phosphate monobasic ($NH_4H_2PO_4$), ammonium metavanadate (NH_4VO_3), trisodium citrate, tetraethyl orthosilicate (TEOS), ethanol, and ammonia aqueous (25 wt%) (Shanghai Chem. Reagent Co.) are all of analytic reagents and were used as supplied. Only distilled water was used.

2.2. Synthesis of Fe_3O_4 nanoparticles

Spherical magnetic Fe_3O_4 nanoparticles were prepared by a modified solvothermal method [19]. Briefly, 1.35 g of $FeCl_3{\cdot}6H_2O$ and 7.2 g of NaAc were dissolved in 40 mL of ethylene glycol. The mixture was stirred vigorously for 30 min at 160 °C to form a homogeneous russet solution, and then transferred into a Teflon lined

* Corresponding author. Tel.: +86 431 85167712.
E-mail address: huayang86@sina.com (H. Yang).

0925-8388/$ – see front matter © 2011 Elsevier B.V. All rights reserved.
doi:10.1016/j.jallcom.2011.08.069

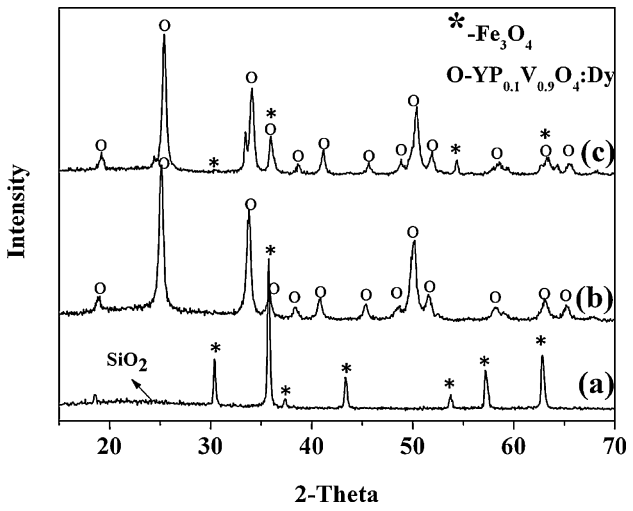

Fig. 1. XRD patterns of Fe_3O_4@SiO_2 (a), $YP_{0.1}V_{0.9}O_4$:Dy^{3+} (b), Fe_3O_4@SiO_2@ $YP_{0.1}V_{0.9}O_4$:Dy^{3+}(c).

stainless-steel autoclave (50 mL capacity). The autoclave was heated to 200 °C and maintained for 8 h. Then it was cooled to room temperature. The black magnetic particles were then rinsed several times with ethanol under ultrasonic conditions to effectively remove the solvent, and dried in vacuum at 60 °C for 12 h.

2.3. Synthesis of Fe_3O_4@SiO_2 nanoparticles

Fe3O4@SiO2 nanoparticles were prepared according to the modified by the Stöber method [20]. Typically, 0.10 g of Fe_3O_4 nanoparticles (~130 nm in diameter) were homogeneously dispersed in a mixture of 40 mL of ethanol, 10 mL of deioned water, and 1.0 mL of 28 wt% concentrated ammonia aqueous solution ($NH_3{\cdot}3H_2O$), followed by the addition of 0.10 g of tetraethyl orthosilicate (TEOS). After vigorous stirring at room temperature for 6 h, the obtained Fe_3O_4@SiO_2 microspheres were separated with a magnet and washed repeatedly with ethanol and water to remove nonmagnetic by products.

2.4. Synthesis of Fe_3O_4@SiO_2@$YP_{0.1}V_{0.9}O_4$:Dy^{3+} nanoparticles

Functionalization of $YP_{0.1}V_{0.9}O_4$:Dy^{3+} on the template free Fe_3O_4@SiO_2 was achieved according to the reported process with the doping concentration of Dy^{3+} of 1 mol% to Y^{3+} in $YP_{0.1}V_{0.9}O_4$:Dy^{3+}[21–23]. Typically, 0.223 g (0.9 mmol) of Y_2O_3, 0.0037 g (0.01 mmol) of Dy_2O_3, 0.023 g (0.2 mmol) $NH_4H_2PO_4$ and 0.2103 g (1.8 mmol) of NH_4VO_3 were dissolved in dilute HNO_3. Then 0.84 g of citric acid (4 mmol) was added as a chelating agent. After stirred for 1 h, a homogenous sol was formed. Then desired amount of treated Fe_3O_4@SiO_2 powders was added into the sol with stirring. After further stirred for another 3 h, the resulting material was dried at 120 °C for 12 h. The obtained material was denoted as Fe_3O_4@SiO_2@$YP_{0.1}V_{0.9}O_4$:Dy^{3+}.

2.5. Characterization

The structure properties of all samples were checked by X-ray diffraction measurements at room temperature using CuKα radiation ($k\alpha$ = 1.54059 Å). A spectrophotometer (Hitachi F-4500 spectrophotometer equipped with a 150 W xenon lamp as the excitation source) was used for the photoluminescent (PL) measurement at room temperature. The morphology and structure of as synthesized composites were characterized with scanning electronic microscope (SEM, Philips XL-30) and transmission electron microscopy (TEM, JEOL Jem-1200EX). The room temperature magnetic hysteresis (M–H) loops were measured using a vibrating sample magnetometry (VSM) system (JDM-13).

3. Results and discussion

Fig. 1 shows the XRD patterns of Fe_3O_4@SiO_2, $YP_{0.1}V_{0.9}O_4$:Dy^{3+} and Fe_3O_4@SiO_2@ $YP_{0.1}V_{0.9}O_4$:Dy^{3+} nanoparticles. The XRD peaks in Fig. 1(a) and (b) can be readily indexed to a face-centered cubic structure of Fe_3O_4@SiO_2 and the tetragonal phase of $YP_{0.1}V_{0.9}O_4$, respectively. In the case of Fe_3O_4@SiO_2@ $YP_{0.1}V_{0.9}O_4$:Dy^{3+}, the peaks marked by asterisk (at 31.2, 36.5, 54.1 and 61) can be indexed to Fe_3O_4 and those marked by circle can be indexed to $YP_{0.1}V_{0.9}O_4$:Dy^{3+}, which are in good agreement with the values in the standard card (JCPDS No.17-341 and 11-254). Therefore, the presence of diffraction peaks can be used to evaluate the structural order at long range or periodicity of the material [25]. All diffraction peaks can be assigned to the cubic, tetragonal and monoclinic structure.

The results reveal that the coexistence of the Fe_3O_4 phase and $YP_{0.1}V_{0.9}O_4$:Dy^{3+} phase in the nanocomposite. For Fe_3O_4@SiO_2 in Fig. 1(a), the broad band at 2θ = 22.0–25.0° can be assigned to the amorphous SiO_2 shell (JCPDS No. 29-0085).

The SEM image shows that magnetite (Fe_3O_4) particles have a mean diameter of about 130 nm and a nearly spherical shape in Fig. 2(a). The magnetite particles coated with hydrophilic species such as a silicon dioxide layer is of great interest to enhance its dispersibility in aqueous solution and prevent them from aggregating in liquid media. In addition, a shell such as the silicon layer can effectively separate lanthanide based photoluminescence component from the magnetite and prevent the luminescence from quenching by magnetite. Fig. 2(b) shows that Fe_3O_4@SiO_2 particles still keep the morphological properties of Fe_3O_4 except for a slightly larger particle size and smoother surface, which silica are uniform coated on the Fe_3O_4 particles to form silica shell. Compared to the Fe_3O_4@SiO_2 microspheres, the Fe_3O_4@SiO_2@ $YP_{0.1}V_{0.9}O_4$:Dy^{3+} nanocomposites have a rougher surface because the $YP_{0.1}V_{0.9}O_4$:Dy^{3+} nanoparticles are randomly deposited on the Fe_3O_4@SiO_2 microspheres, as shown in the SEM image (Fig. 2(c)). The rough surface may provide a higher specific area and be more beneficial for the biological application. Fig. 2(d) shows the TEM image of the Fe_3O_4@SiO_2@$YP_{0.1}V_{0.9}O_4$:Dy^{3+} nanocomposites obtained by modified treatment of Fe_3O_4@SiO_2 microspheres by sol–gel process, from which a grey layer (~25 nm in thickness) deposited by numerous $YP_{0.1}V_{0.9}O_4$:Dy^{3+} nanoparticles can be clearly seen on the magnetite particles' surface. These nanocomposites also have the bigger particle sizes and less aggregation, which can be seen clearly in Fig. 3. The size may be up to about 500 nm as the mass ration of core/shell is 1:6.

The photoluminescence properties of $YP_{0.1}V_{0.9}O_4$:Dy^{3+} and Fe_3O_4@SiO_2@$YP_{0.1}V_{0.9}O_4$:Dy^{3+} were further characterized by the excitation spectra and emission spectra in Fig. 4. In the excitation spectra (Fig. 4(A)), the strong excitation band of the samples is at about 325 nm at the emission wavelength of 573 nm, which is ascribed to a charge transfer from the oxygen ligands to the central vanadium atom insides the VO_4^{3-} group ions. In the emission spectra of samples (Fig. 4(B)), the characteristic transition lines from the lowest excited $^4F_{9/2}$ level of Dy^{3+} to $^6H_{15/2}$ and $^6H_{13/2}$ are observed, dominated by the $^4F_{9/2}$–$^6H_{13/2}$ hypersensitive transition (ΔJ = 2). It is because the Dy^{3+} ions in the YVO_4 host lattices are located at a low symmetry local site D_{2d} without inversion center in the YVO_4 host lattices [24]. Moreover, the presence of the VO_4^{3-} absorption in the excitation spectrum of Dy^{3+} indicates that an energy transfer occurs from VO_4^{3-} ions to Dy^{3+} ions in YVO_4:Dy^{3+}, and the energy transfer is very efficient because the emission of VO_4^{3-} is not observed and only the emission of Dy^{3+} is observed upon excitation at the VO_4^{3-}. The energy transferring from VO_4^{3-} to Dy^{3+} is dominated by exchange interaction at room temperature like VO_4^{3-}–Dy^{3+} energy transfer in YVO_4 [22]. Although the silica matrix acts as a barrier to protect $YP_{0.1}V_{0.9}O_4$:Dy^{3+} from quenching completely, Fe_3O_4 also products some effects to a certain extent. Thus the intensities of both the excitation spectra and emission spectra of Fe_3O_4@SiO_2@$YP_{0.1}V_{0.9}O_4$:Dy^{3+} are decreased. Indeed, Fe_3O_4@SiO_2@$YP_{0.1}V_{0.9}O_4$:Dy^{3+} colloidal solution is exhibited yellow-green PL emission at room temperature under a UV-light in the inset of Fig. 3(b).

Fig. 5 gives the excitation spectra and emission spectra of bifunctional nanocomposites with the different mass ration of core/shell. It is clear that both the excitation spectra and emission spectra

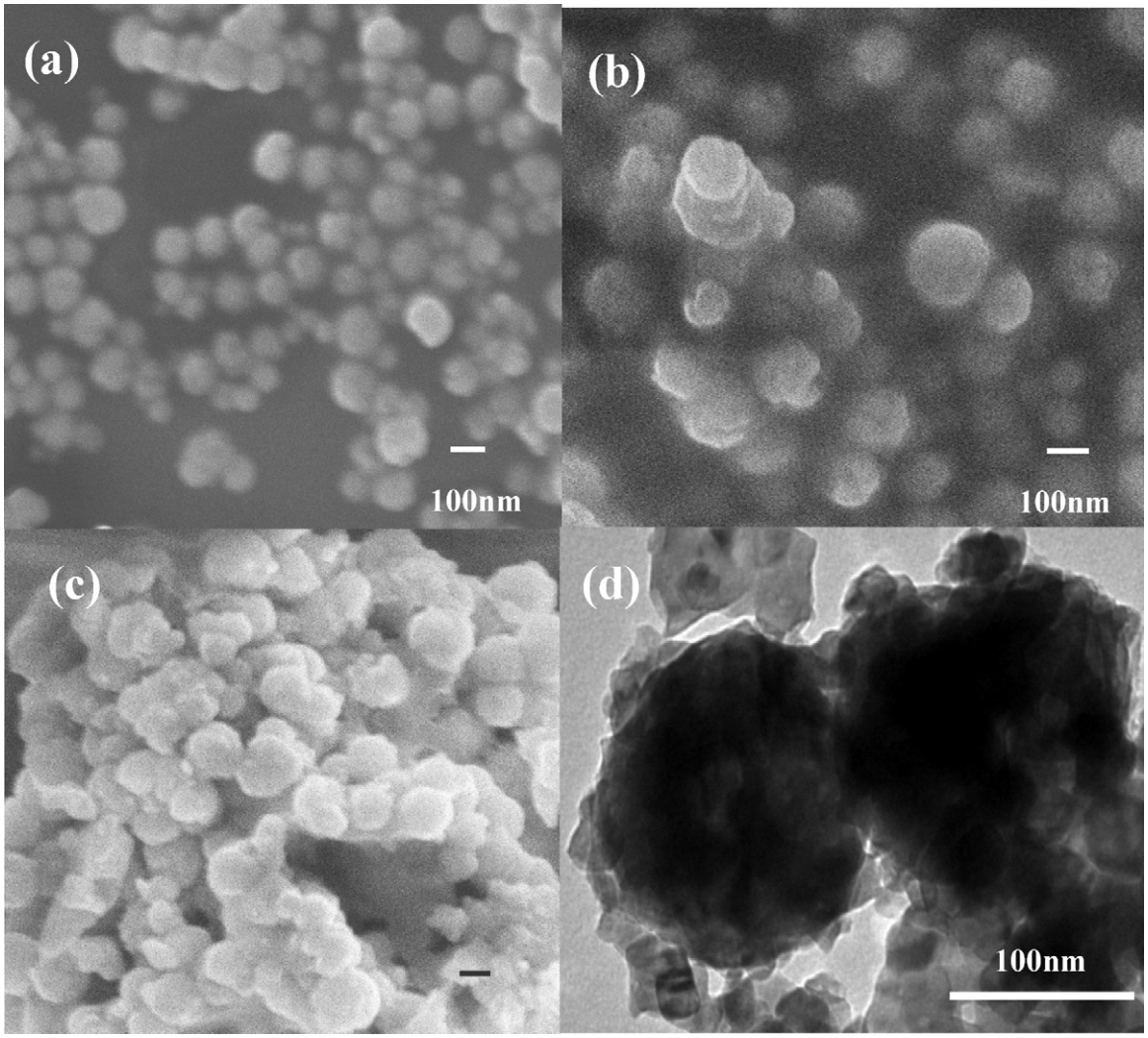

Fig. 2. SEM images of Fe_3O_4 (a), Fe_3O_4@SiO_2 (b), Fe_3O_4@SiO_2@$YP_{0.1}V_{0.9}O_4$:Dy^{3+} (c) and TEM images of Fe_3O_4@SiO_2@$YP_{0.1}V_{0.9}O_4$:Dy^{3+} (d).

bands grow stronger with decreasing the mass ration of core/shell. Moreover, the particle size may be up to about 500 nm as the mass ration of core/shell is 1:6 in Fig. 3. Unfortunately, the relative strong luminescence always accompanies with the weak magnetism. When the mass ration of core/shell is 1:4, there are the excellent luminescence and magnetism of Fe_3O_4@SiO_2@$YP_{0.1}V_{0.9}O_4$:Dy^{3+}.

Fig. 6 shows the magnetic hysteresis loops of Fe_3O_4, Fe_3O_4@SiO_2 and Fe_3O_4@SiO_2@$YP_{0.1}V_{0.9}O_4$:Dy^{3+} nanocomposites. The special saturation magnetization Ms of Fe_3O_4 nanoparticle is 73 emu g^{-1} in Fig. 6(a), which is closely related to their particle size of samples. The Ms value of Fe_3O_4@SiO_2 is decreased to 68 emu g^{-1} in Fig. 6(b). After $YP_{0.1}V_{0.9}O_4$:Dy^{3+} is coated on the of Fe_3O_4@SiO_2, the special

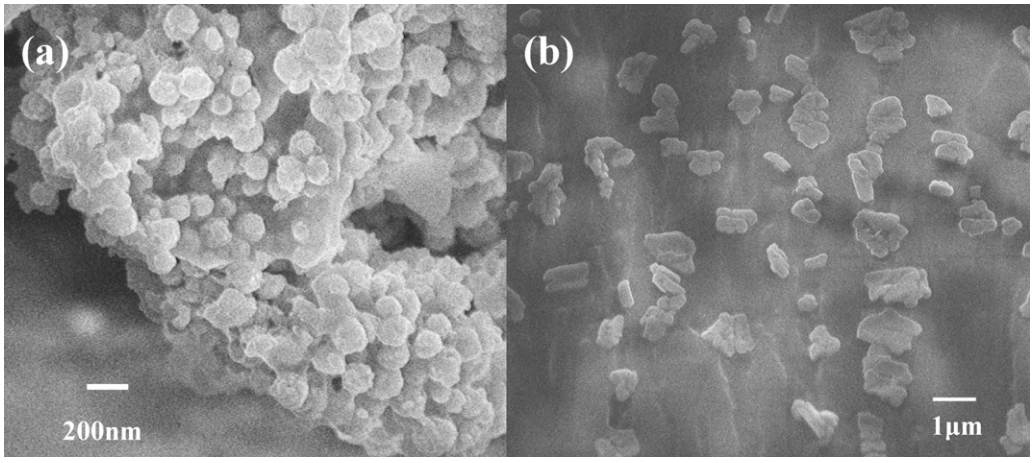

Fig. 3. SEM images of Fe_3O_4@SiO_2@$YP_{0.1}V_{0.9}O_4$:Dy^{3+} which molar ration of core/shell are 1:2(a) 1:6(b).

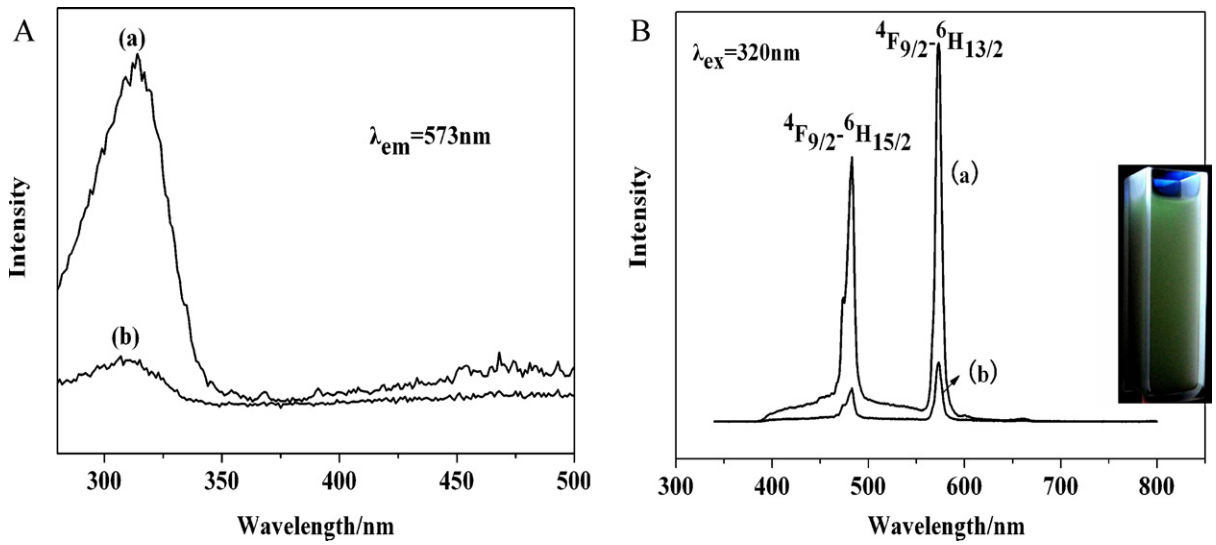

Fig. 4. Excitation spectra (A) and emission spectra (B) of $YP_{0.1}V_{0.9}O_4$:Dy^{3+} (a) and Fe_3O_4@SiO_2@$YP_{0.1}V_{0.9}O_4$:Dy^{3+} (b).

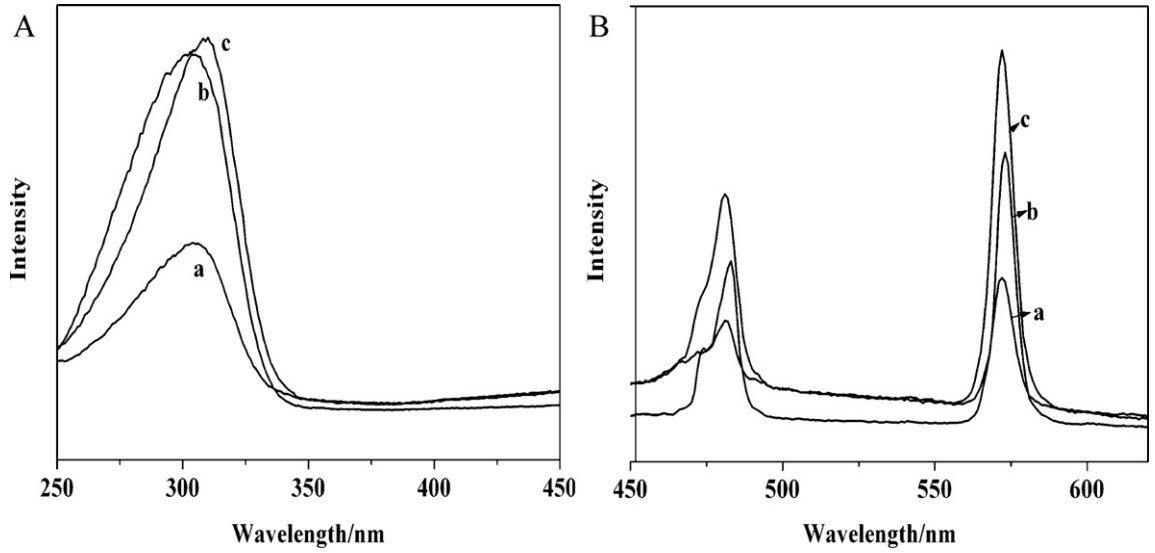

Fig. 5. Excitation spectra (A) and emission spectra (B) of Fe_3O_4@SiO_2@$YP_{0.1}V_{0.9}O_4$:Dy^{3+} which mass ration of core/shell are 1:2(a), 1:4(b) and 1:6(c).

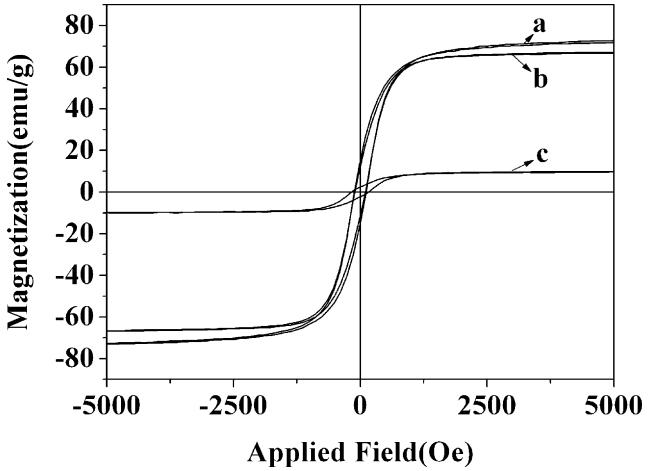

Fig. 6. The magnetic hysteresis loops of Fe_3O_4 (a), Fe_3O_4@SiO_2 (b), Fe_3O_4@SiO_2@$YP_{0.1}V_{0.9}O_4$:Dy^{3+} (c), nanocomposites.

saturation magnetization Ms of Fe_3O_4@SiO_2@$YP_{0.1}V_{0.9}O_4$:Dy^{3+} nanocomposites is significantly decreased to 10 emu g^{-1} (Fig. 6(c)). This phenomenon was mainly caused by the presence of high proportion of $YP_{0.1}V_{0.9}O_4$:Dy^{3+} in the composite NPs. Fortunately, the magnetism of as-synthesized Fe_3O_4@SiO_2@ $YP_{0.1}V_{0.9}O_4$:Dy^{3+} nanocomposites fulfils the requirements for bioseparation and enrichment.

Fig. 7 shows the excitation spectra and emission spectra of Fe_3O_4@SiO_2@$YP_{0.1}V_{0.9}O_4$:Dy^{3+} nanocomposites dealt under the external magnetic fields. The effects of the magnetic field on the photoluminescence intensity of the nanocomposite were discussed. The Fe_3O_4@SiO_2@$YP_{0.1}V_{0.9}O_4$:Dy^{3+} was under the magnetic fields 0.25 T for 1 h, 2 h, 3 h, 4 h and 5 h respectively. From Fig. 7, the photoluminescence intensities of the nanocomposite are firstly increased with increasing the time, and then decreased. When for 3 h, there is a highest photoluminescence intensity. The possible interpretation was discussed in Scheme 1. When the external magnetic fields took effect on the magnetic silica, the magnetic energy was partly transferred to the magnetic silica and the rest released in the form of heat. It was represented that the energy of the valence electron of the magnetite increased so that the valence

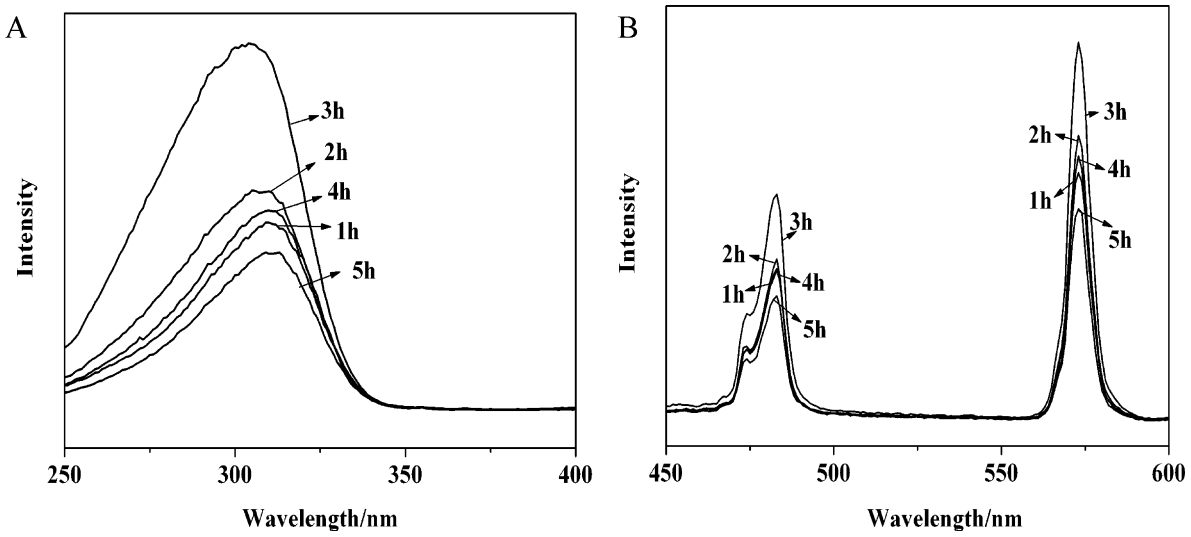

Fig. 7. Excitation (A) spectra and emission spectra (B) of Fe_3O_4@SiO_2@$YP_{0.1}V_{0.9}O_4$:Dy^{3+} under the external magnetic field for 1 h, 3 h, 4 h and 5 h.

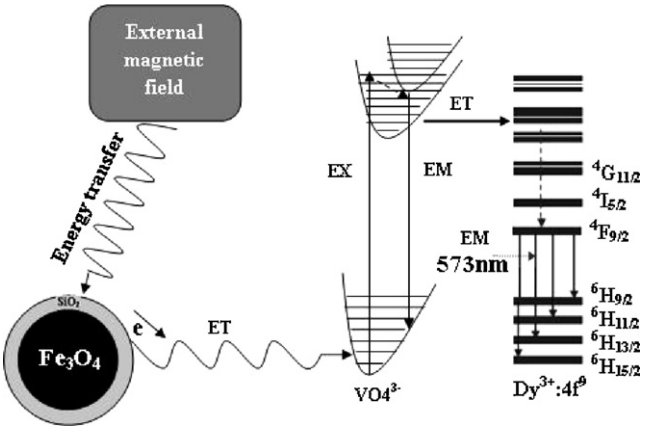

Scheme 1. The possible action mechanism under the magnetic field on the luminescence intensity of the nanocomposite.

electron tended to escape from the orbit, but the system gave a restriction on the valence electron to keep it steady. And then the energy was transferred from the valence electron of magnetite to that of phosphors. However, with the plus action time (up to 3 h) under magnetic field, the increased energy showed the opposite effect. As a result, the valence electron of magnetite became steady and no longer transfer energy to phosphor, so the fluorescence intensity of phosphors decreased. The other reason may be the form of the lattice defects which result in the changing of magnetism and then further affect the photoluminescence intensity. During the excitation process at room temperature, the electrons situated at lower intermediary energy levels (oxygen 2p states) absorb the photon energies ($h\nu$) arising from different wavelengths. As consequence of this phenomenon, the energetic electrons are promoted to higher intermediary energy levels (vanadium 3*d* states) located near the conduction band. When the electrons fall back to lower energy states again via radiative return processes, the energies arising from this electronic transition are converted in photons ($h\nu'$). In this case, the several photons ($h\nu'$) originated by the participation of different energy states during the electronic transitions are responsible for the broad PL spectra.

4. Conclusion

In conclusion, we report the facile synthesis of a novel magnetic/photoluminescence bifunctional nanocomposites Fe_3O_4@SiO_2@$YP_{0.1}V_{0.9}O_4$:Dy^{3+} nanocomposites with core–shell structure by the solvothermal method and sol–gel method. The as-prepared bifunctional nanocomposites combined the advantages of magnetism and photoluminescence, The obtained Fe_3O_4@SiO_2@$YP_{0.1}V_{0.9}O_4$:Dy^{3+} nanocomposites have a mean diameter of 180 nm and uniform $YP_{0.1}V_{0.9}O_4$:Dy^{3+} shell (about 25 nm in thickness). From the effects of the magnetic field on the photoluminescence intensity, it is shown that the photoluminescence intensities are gradually increased with the action time until the duration was 3 h, and then gradually decreased. The double matrix and bifunctional nanocomposites may be a potential materials application in more biological fields.

Acknowledgment

This work is supported by the National Natural Science Foundation of China (NSFC).

References

[1] P. Sharrna, S. Brown, G. Walter, S. Santra, B. Moudgil, Adv. Colloid Interface Sci. 123 (2006) 471;
W.H. Tan, K.M. Wang, X.X. He, X.J. Zhao, T. Drake, L. Wang, R.P. Bagwe, Med. Res. Rev. 24 (2004) 621.
[2] M. De, P.S. Ghosh, V.M. Rotello, Adv. Mater. 20 (2008) 4225.
[3] J.H. Gao, B. Zhang, Y. Gao, Y. Pan, X.X. Zhang, B. Xu, J. Am. Chem. Soc. 129 (2007) 11928;
J.-H. Lee, B. Schneider, E.K. Jordan, W. Liu, J.A. Frank, Adv. Mater. 20 (2008) 2512;
M. Liong, J. Lu, M. Kovochich, T. Xia, S.G. Ruehm, A.E. Nel, F. Tamanoi, J.I. Zink, ACS Nano 2 (2008) 889;
K.S. Iyer, M. Saunders, T. Becher, C.W. Evans, C.L. Raston, J. Am. Chem. Soc. 131 (2009) 16338.
[4] H.W. Gu, R.K. Zheng, X.X. Zhang, B. Xu, J. Am. Chem. Soc. 126 (2004) 5664;
D.S. Wang, J.B. He, N. Rowenzweig, Z. Rosenzweig, Nano Lett. 4 (2004) 409.
[5] F. Bertorelle, C. Wilhelm, J. Roger, F. Gazeau, C. Menager, V. Cabuil, Langmuir 22 (2006) 5385;
S.S. Banerjee, D.H. Chen, Nanotechnology 20 (2009) 185103.
[6] Z.Y. Ma, D. Dosev, M. Nichkova, S.J. Gee, B.D. Hammock, I.M. Kennedy, J. Mater. Chem. 19 (2009) 4695.
[7] J. Fang, M. Saunders, Y. Guo, G. Lu, C.L. Raston, K.S. Iyer, J. Am. Chem. Soc. 122 (2000) 9692.
[8] H. Mattoussi, J.M. Mauro, E.R. Goldman, G.P. Anderson, V.C. Sundar, F.V. Mikulec, M.G. Bawendi, J. Am. Chem. Soc. 122 (2000) 12142;
W.C.W. Chan, S.M. Nie, Science 281 (1998) 2016.
[9] J.K. Jaiswal, H. Mattoussi, J.M. Mauro, S.M. Simon, Nat. Biotechnol. 21 (2003) 47;
B. Dubertret, P. Skourides, D.J. Norris, V. Noireaux, A.H. Brivanlou, A. Libchaber, Science 298 (2002) 1759.
[10] R. Hardman, Environ. Health Perspect. 114 (2006) 165;
A.M. Derfus, W.C.W. Chan, S.N. Bhatia, Nano Lett. 4 (2004) 11.
[11] Y.X. Zhang, G.K. Das, R. Xu, T.T.Y. Tan, J. Mater. Chem. 19 (2009) 3696.

[12] F. Wang, W.B. Tan, Y. Zhang, X. Fan, M. Wang, Nanotechnology 17 (2006) 1527.
[13] L.Y. Wang, R.X. Yan, Z.Y. Huo, L. Wang, J.H. Zeng, J. Bao, X. Wang, Q. Peng, Y.D. Li, Angew. Chem. Int. Ed. 44 (2005) 6054.
[14] H.C. Lu, G.S. Yi, S.Y. Zhao, D.P. Chen, L.-H. Guo, J. Cheng, J. Mater. Chem. 14 (2004) 1336.
[15] D. Dosev, M. Nichkova, R.K. Dumas, S.J. Gee, B.D. Hammock, K. Liu, I.M. Kenne, Nanotechnology 18 (2007) 055102.
[16] J. Fang, M. Saunders, cY. Guo, G. Lu, C.L. Raston, K.S. Iyer, Chem. Commun. 46 (2010) 3074.
[17] P.P. Yang, Z.W. Quan, Z.Y. Hou, C.X. Li, X.J. Kang, Z.Y. Cheng, J. Lin, Biomaterials 30 (2009) 4786.
[18] E.V. Groman, J.C. Bouchard, C.P. Reinhardt, D.E. Vaccaro, Bioconjug. Chem. 18 (2007) 1763;
C.R. De Silva, S. Smith, I. Shim, J. Pyun, T. Gutu, J. Jiao, Z. Zheng, J. Am. Chem. Soc. 131 (2009) 6336;
S.Y. Yu, H.J. Zhang, J.B. Yu, C. Wang, L.N. Sun, W.D. Shi, Langmuir 23 (2007) 7836.
[19] X.Q. Xu, C.H. Deng, M.X. Gao, W.J. Yu, P.Y. Yang, X.M. Zhang, Adv. Mater. 18 (2006) 3289.
[20] W. Stöber, A. Fink, E. Bohn, J. Colloid Interface Sci. 26 (1968) 62.
[21] M.P. Pechini, Method of preparing lead and alkaline earth titanates and niobates and coating method to form a capacitor, US Patent no. 3,330,697; 1967.
[22] A. Bao, H. Yang, C.Y. Tao, Y. Zhang, L.L. Han, J. Lumin. 128 (2008) 60.
[23] E. Cavalli, M. Bettinelli, A. Belletti, A. Speghini, J. Alloys Compds. 341 (2002) 107.
[24] J.M. Nedelec, D. Avignant, R. Mahiou, Chem. Mater. 14 (2002) 651.
[25] L.S. Cavalcante, V.S. Marques, J.C. Sczancoski, M.T. Escote, M.R. Joya, J.A. Varela, M.R.M.C. Santos, P.S. Pizani, E. Longo, Chem. Eng. J. 143 (2008) 299–307.